Soft Matter

RSC Publishing

PAPER

Squeezing particle-stabilized emulsions into biliquid foams – equation of state†

Cite this: *Soft Matter*, 2013, **9**, 7757

Louison Maurice,‡ Ryan A. Maguire, Andrew B. Schofield, Michael E. Cates, Paul S. Clegg and Job H. J. Thijssen*

Using a centrifuge, we measure the (pressure *vs.* density) equation of state of Pickering emulsions stabilized by hard-sphere colloids, in order to elucidate the particle contribution to their mechanical properties. Moreover, we have developed a transparent Pickering emulsion, allowing us to determine local volume fraction as a function of distance within the sediment using confocal microscopy, thus extracting an entire equation of state from one centrifugation cycle. We can explain and predict trends in our data using a quantitative model incorporating interdroplet films with a thickness on the scale of the (micron-sized) particles and repulsive interactions across these films. We suggest that the effective repulsion between droplets is due to the deformation of the liquid–liquid interface between particles on one droplet due to compression against a neighbouring droplet.

Received 16th April 2013
Accepted 27th June 2013

DOI: 10.1039/c3sm51046h

www.rsc.org/softmatter

1 Introduction

Designing soft composites requires predictive control of their morphology and mechanical properties.[1–3] An intriguing class of soft composites consists of emulsions/foams, *i.e.* dispersions of droplets/bubbles in an immiscible liquid, because they can display solid-like behavior despite being comprised of fluids.[2] Such materials are ubiquitous in *e.g.* the food, personal-care and petrochemical industries.[4] Recent years have seen a growing interest in emulsions/foams stabilized by colloidal particles rather than molecular surfactants, mainly because they feature superior functionality and shelf life.[3–6] Unlike their molecular counterparts, particulate emulsifiers can become irreversibly attached to droplet surfaces by reducing energy–expensive liquid–liquid contact area. This is described by

$$\Delta G_{\mathrm{d}} = \pi r^2 \gamma (1 \pm \cos(\theta))^2 \qquad (1)$$

where γ is the liquid–liquid interfacial tension and ΔG_{d} is the free energy of detachment for a spherical particle of radius r and contact angle θ; the sign inside the bracket is negative for removal into the water phase and positive for removal into the oil phase.[6] Note that $\Delta G_{\mathrm{d}} \sim 4 \times 10^4\ k_{\mathrm{B}}T_0$ for detachment of a hydrophobic particle with radius $r \sim 0.5$ μm into the oil phase, even for a contact angle as high as $\theta \sim 160^\circ$ (Boltzmann constant k_{B}; room temperature T_0; θ measured through the water phase).[7,8] These particle-stabilized, or Pickering–Ramsden (PR), emulsions/foams also feature in the rational design of porous materials, including 'colloidosomes'[9] and macrocellular foams.[10]

The mechanical properties of PR emulsions are not yet fully understood, for they arise from a rich interplay between the elasticity of the liquid–liquid interface and interparticle interactions.[11–14] Traditional studies tend to focus on shear, though it has recently been suggested that osmotic compression can play a pivotal role in the rheology of complex fluids, *e.g.* the impact resistance of cornflour.[15] Similarly, the compression of PR emulsions has been left relatively neglected (particularly in the case of model particles).[13,16–19] Knowing the (pressure *vs.* density) equation of state of well-defined PR emulsions would lead to an understanding of their behavior in mechanical equilibrium, which is essential in interpreting non-equilibrium (shear-rheological) experiments on similar samples. Furthermore, a comprehensive investigation could elucidate the specific contribution of the particulate stabilizer to the morphology and mechanical properties of particle-stabilized liquid–liquid composites, which is essential to their further processing and use, *e.g.* as scaffolds for technologically relevant porous materials,[14] and for shelf life.[20]

Here, we measure the equation of state of water-in-oil (w/o) PR emulsions *via* centrifugal compression and we interpret our results using a quantitative model adapted from surfactant-stabilized emulsions.[21,22] To facilitate data interpretation, we initially consider standard (opaque) PR emulsions. However, we also present a (compound) transparent PR emulsion and use confocal microscopy to determine the local volume fraction as a function of distance within the sediment, thus extracting an entire equation of state from one centrifugation cycle. Crucially, we employ colloidal particles that interact as hard spheres in the continuous oil phase due to steric stabilization,[23,24] *i.e.*

SUPA, School of Physics & Astronomy, The University of Edinburgh, Edinburgh, EH9 3JZ, UK. E-mail: j.h.j.thijssen@ed.ac.uk

† Electronic supplementary information (ESI) available. See DOI: 10.1039/c3sm51046h

‡ Current address: École Normale Supérieure de Lyon, Université Claude Bernard Lyon I, Lyon, France.

polymer chains grafted onto their surface.[25] At low droplet volume fractions Φ, near the random close packing threshold for spheres (RCP), our results agree with literature data for emulsions stabilized by molecular surfactants or flocculating nanoparticles.[13,22,26–28] New behavior emerges on increasing Φ, where the osmotic pressure Π of our PR emulsions increases more rapidly. We attribute this to (1) finite-thickness inter-droplet films and (2) an (effective) repulsion between droplet facets, which we argue to be due to the deformation of the liquid–liquid interface between particles on one droplet upon compression against a neighbouring droplet.

The rest of this paper is organized as follows. In Section 2, we describe the experimental procedures, including sample preparation, centrifugal compression and characterization techniques. Subsequently, in Section 3, we calculate the expected (pressure *vs.* density) equation of state by adapting a quantitative model from surfactant-stabilized emulsions. In Section 4, we present the measured equation of state of both standard and transparent PR emulsions, after which we discuss its interpretation in Section 5 together with incomplete post-centrifugation recovery and materials-science aspects. Finally, in Section 6, we summarize our findings and draw conclusions.

2 Materials and methods

2.1 Sample preparation

2.1.1 Standard (opaque) emulsions. Standard (opaque) samples were prepared with water, oil and poly(methyl methacrylate) (PMMA) spheres. Water was distilled and passed through a Millipore Milli-Q RG system (resistivity 18 MΩ cm), whereas the oil *n*-dodecane was used as received (Sigma-Aldrich, ≥99%). The PMMA particles, stabilized by a layer of poly(12-hydroxystearic acid) (PHSA), were synthesized following Bosma *et al.*[23] They were fluorescently labeled with 4-chloro-7-nitrobenzo-2-oxa-1,3-diazol (NBD), which was chemically linked to the PMMA during particle synthesis. Following Thijssen *et al.*,[7] particles were cleaned by repeated (10×) centrifugation/redispersion in hexane or dodecane, after which they were dried under vacuum in an oven at (43 ± 3) °C. According to static light scattering, they had a radius $r = 0.630$ μm and a polydispersity pd = 9%.

Sample mixtures were prepared at fixed water/oil volume ratios of 40/60 and overall colloid volume fractions of 1.8 to 4.3% (ESI, Table 1†) in ∼7.5 cm long, cylindrical glass vials of internal cross-section $A = (2.574 \pm 0.019)$ cm^2. The dried colloids were dispersed in *n*-dodecane using an 80 W ultrasonic bath (VWR) for at least (3 × 15) min, each cycle followed by 30 s of vortex mixing (Fisons). Subsequently, water was added and the samples were emulsified by cycles comprising 30 s of vortex mixing followed by 2.5 min of rest (repeated till the supernatant was clear).[7] After preparation, the samples were left to sediment for up to 48 h, during which time they were frequently tapped to promote random close packing.[29] A small fraction of sediment was carefully extracted for microscopy, for which we corrected the droplet volume fraction by assuming that the mass removed had the density of an emulsion after sedimentation.

All amounts were determined by weighing; volume fractions were calculated using the densities of PMMA ($\rho_p = (1.166 \pm 0.052)$ g mL^{-1}),[30] *n*-dodecane ($\rho_o = (0.7460 \pm 0.0015)$ g mL^{-1})[31] and water ($\rho_w = (0.99696 \pm 0.00011)$ g mL^{-1}) (density meter, Anton Paar, DMA 4500).

2.1.2 (Compound) transparent emulsions. For 3D confocal imaging, we developed a *transparent* system containing the same PMMA particles. A mixture of poly(dimethylsiloxane-*co*-methylphenylsiloxane) (DC550, Aldrich, Dow Corning 550®fluid) and cycloheptyl bromide (CHB, Aldrich, 97%) was used as the oil phase (DC550 : CHB = 83 : 17 v/v). The aqueous phase was a 65 wt% solution of sodium iodide (Sigma-Aldrich, ≥99.5%) in de-ionized water. To allow separate imaging of the oil phase, the CHB was saturated with Nile Red (Sigma, technical grade), an uncharged fluorescent dye that does not act as a surfactant.[7,32] An Abbe refractometer was used to measure the refractive index of the oil and aqueous phases, which were 1.498 and 1.496 respectively, closely matching the refractive index of the PMMA particles (1.503). The densities were determined to be 1.103 g mL^{-1} (oil) and 1.881 g mL^{-1} (aqueous).

Sample mixtures were prepared in ∼7 mL cylindrical glass vials at fixed volume ratios of 40/60 aqueous/oil phase and overall colloid volume fractions of 0.9 to 4.0%. The dried colloids were dispersed in the oil phase using the 80 W ultrasonic bath and the vortex mixer. A minimum of 3 sonication cycles of 30 minutes, each followed by 30 s of vortex mixing, was required to achieve good dispersion of PMMA within the oil phase (verified by confocal microscopy). After addition of the aqueous phase, samples were emulsified *via* two 30 s cycles of vortex mixing. After preparation, approximately 0.4 mL of each emulsion was carefully transferred by Pasteur pipette from the vials to glass cuvettes (Starna, 10 × 30 mm^2, path length 1 mm). The samples were then left overnight to settle.

2.2 Compression and expansion

To measure their equation of state, standard samples were compressed for at least 8 hours in a swinging-bucket centrifuge (Denley BS400) (Fig. 1); we checked that mechanical equilibrium had been reached after 8 h by centrifuging some samples for ∼63 h. Angular velocities were calibrated using a digital photo tachometer (Lutron DT-2236) and ranged from $0 \leq \omega \leq 332$ rad s^{-1}. The distance between the centrifugal axis and the outside bottom of the vials was measured using a vernier caliper (Mitutoyo): $d_c = 13.8 \pm 0.5$ cm; the main contribution to the error coming from the potential compression of the semi-spherical silicone-rubber adapters that had been inserted into the buckets to protect the vials from shattering.

As the centrifugal pressure acts as a 'virtual' semi-permeable membrane squeezing the oil out of the droplet sediment, the pressure required in mechanical equilibrium to prevent the continuous phase from being sucked back in can be interpreted as an osmotic pressure Π,[17,33]

$$\Pi(\delta) = (\rho_d - \rho_o)\omega^2\delta \int_{d_c-H}^{d_c} \Phi(\delta')\mathrm{d}\delta', \quad (2)$$

in which $\rho_d(\rho_o)$ is the density of the particle-laden droplets (continuous oil phase) and ω is the angular frequency of the centrifuge. If the height of the sediment H is much smaller than

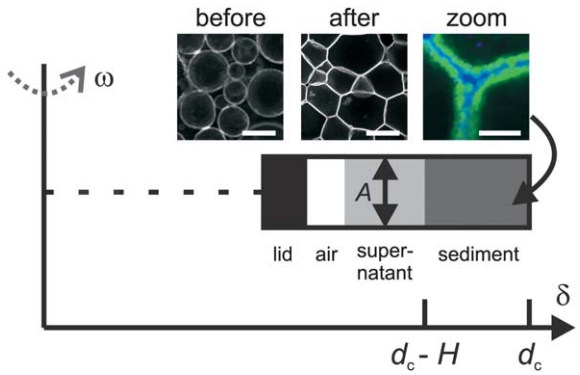

Fig. 1 Centrifuge schematic: angular frequency ω, lever arm d_c, emulsion-sediment height H and cross-section A. Insets: confocal micrographs of water-in-dodecane (blue) emulsions, stabilized by PMMA particles (white/green), before and after centrifugation at 522g; scale bars 100 μm (362g and 10 μm for zoom).

the centrifuge lever arm d_c (here $H/d_c \sim 2.8$ cm/13.8 cm – ref. 34)), the spatial gradient in both Φ and the centrifugal acceleration $a_c = \omega^2\delta$ can be neglected, *i.e.* $\Pi \simeq \Pi(d_c - (H/2))$,[13,17]

$$\Pi = (\rho_d - \rho_o)\omega^2 \Phi H\left(d_c - \frac{H}{2}\right). \quad (3)$$

After compression, the overall droplet volume fraction Φ of the emulsion sediment was calculated from H using

$$\Phi = \frac{V_w + V_p}{AH}, \quad (4)$$

in which $V_w(V_p)$ is the volume of the water (particles). As the tops of the sediments were sometimes slanted, we measured H at 8 positions around the vial using a mounted dial ruler. To correct for emulsion recovery, we used a camera to monitor the post-centrifugation change in sediment height ΔH and subtracted it from H_{final} (see ESI Section 7 for detailed recovery analysis†). After recovery, samples were either re-emulsified (ESI Section 5†) or centrifuged at higher ω (Fig. 4), leading to similar results.

In the case of transparent samples, compressive stress was applied by centrifugation for 16 h at ~263g (≡ 874g for standard samples due to density differences); no substantial differences were observed when using a different centrifuge (Heraeus Multifuge 3SR Plus). To protect the cuvettes from shattering during centrifugation, they were inserted into silicone-rubber adapters (d_c = 12 cm). After centrifugation, the sediment height was monitored every 5 min for 24 h using a Labview-controlled webcam (Logitech), but no noticeable expansion was observed in these samples. This allowed for 3D characterization of their morphology using confocal fluorescence microscopy (see below).

2.3 Sample characterization

To provide microscopic explanations for our macroscopic observations, standard emulsions were transferred to glass cuvettes. To check that the transfer did not affect the samples, we also prepared and centrifuged samples in square glass cuvettes (1 cm path length), *i.e.* without transfer. Both before and after centrifugation, they were imaged at various locations along the cuvette, from the inner glass wall up to depths of ~100 μm, using a Zeiss Observer.Z1 inverted microscope in conjunction with a Zeiss LSM700 confocal scanning unit. A 488 nm diode laser was used to excite NBD in PMMA and Nile Red in *n*-dodecane, while a 555 nm diode laser was employed for $DiIC_{18}$ in PMMA (only Fig. 7); filters were used as appropriate. In samples with two fluorescent dyes, lines were scanned sequentially to minimize cross-talk between the two channels. Image signal-to-noise was enhanced by averaging (1 to 4×). Owing to the 1.25 mm glass walls of the cuvettes, required to withstand centrifugal pressures, long-working-distance objectives were used: Zeiss LD Plan-Neofluar 20×/0.4NA and LD Plan-Neofluar 63×/0.75NA (both with a correction collar).

In the transparent samples (already in cuvettes), the Nile Red in the oil phase or the Rhodamine B in the PMMA (only Fig. 7) was excited with a 555 nm laser. 3D image series were captured at a minimum of 7 positions along the radial axis (δ in Fig. 1), at a depth between 100 μm and 400 μm, using a Zeiss LD Plan-Neofluar 20×/0.4NA or 40×/0.6NA objective. To minimize out-of-focus contributions, the confocal pinhole aperture was made as small as possible, while maintaining signal-to-noise by averaging (2×).

For further details regarding emulsion characterization, including interfacial-tension measurements, droplet sizing, particle specific surface area and image analysis, see ESI Section 3†.

3 Theory

One of the distinctive features of our system is that the particles should behave as hard spheres under ambient conditions,[23,24] which helps model their contribution to the equation of state. Here we follow a model by Buzza and Cates,[21] starting with a 3D array of spherical, close-packed, monodisperse water droplets at volume fraction $\phi_0 = 0.7405$. Focussing on one representative droplet, its free energy F upon deformation is

$$F(\Phi, h) = \gamma S(\phi) + \left(\frac{v(h)}{2}\right) S_f(\phi), \quad (5)$$

in which $S(S_f)$ is the droplet surface area (interdroplet film area), $v(h)$ is the repulsion energy per unit area of two flattened surfaces across an interdroplet film of thickness h, and ϕ is the "effective volume fraction",

$$\phi(\Phi, h) = \frac{\Phi}{\left(1 - (\Phi/\phi_0)^{1/3}\left((h - h_p)/2R\right)\right)^3}, \quad (6)$$

i.e. the volume fraction the same droplet would occupy at zero film thickness ($h_p = 0$ for now). To account for polydispersity, we equate the droplet radius R to the Sauter mean droplet radius R_{32} ($R = R_{32}$).[33] The equation of state $\Pi(\Phi)$ can then be obtained using

$$\Pi(\Phi) = \left(\frac{\Phi^2}{V_0}\right)\left(\frac{\partial F}{\partial \Phi}\right)_{V_0}, \quad (7)$$

with constant droplet volume V_0.

Evaluation of eqn (7) requires explicit expressions for $S(\phi)$ and $S_f(\phi)$. Here we start with (empirical) expressions found by Princen and Kiss for surfactant-stabilized emulsions,[22]

$$\frac{S(\phi)}{S_0} = \begin{cases} 1 + \frac{1}{3}\left(\frac{0.084}{\phi} - \frac{0.068}{\phi}\ln(1-\phi) - 0.237\right) \\ \text{for } 0.715 < \phi < 0.90 \\ \left(\frac{0.00283}{1 - 0.9639\phi}\right) + 0.989 \\ \text{for } 0.90 < \phi < 0.99 \\ 0.0686\left(1 - 1.892\sqrt{1-\phi}\right)^3 + 1.014 \\ \text{for } 0.99 < \phi < 1 \end{cases} \quad (8)$$

and

$$S_f = \frac{S_1}{\phi^{2/3}} f(\phi), \quad (9)$$

with

$$\begin{cases} f(\phi) = 1 - \left(\frac{3.20}{\sqrt{(\phi/(1-\phi)) + 7.70}}\right) \\ \text{for } 0.718 < \phi < 0.975 \\ f(\phi) = \left(1 - 1.892\sqrt{1-\phi}\right)^2 \\ \text{for } 0.975 < \phi < 1. \end{cases} \quad (10)$$

Here S_0 and S_1 are the droplet surface areas in the uncompressed and fully compressed states ($S_1 \approx 1.083 S_0$). Combining eqn (5)–(10) for $h = 0$ leads to the solid line in Fig. 2 labelled 'LL'.

Inspired by confocal micrographs (Fig. 1 zoom), we account for the particles by introducing an interdroplet film of thickness h, which causes Φ_{max} to shift to a lower value (lines labelled '+F(F)' in Fig. 2). Note that h is measured between liquid–liquid interfaces across the film, so we subtract from h a thickness h_p corresponding to the volume of particles that resides in the film but should be counted as part of the droplet (eqn (4) and ESI Section 8†). Setting $h_p = 0$ would result in a substantial part of the particles being counted as continuous rather than as droplet phase ($\theta \sim 160°$).

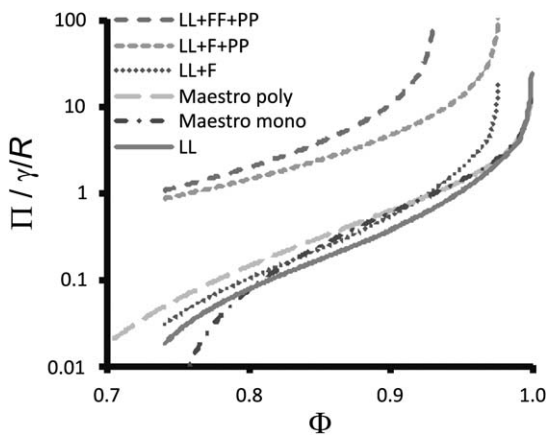

Fig. 2 Calculated osmotic pressure Π *vs.* droplet volume fraction Φ for emulsions with mean droplet radius $R = 67$ μm (LL: $h = 0$ and $\alpha = 0$), including interdroplet films of finite thickness h (+F: $h = 2.4$ μm and +FF: $h = 4.4$ μm) and including repulsive interactions (+PP: $\alpha = 1$ rather than $\alpha = 0$); γ is the liquid–liquid interfacial tension. Curves to compare monodisperse and polydisperse emulsions (for $h = 0$ and $\alpha = 0$) have been calculated following Maestro *et al.*[28]

Subsequently, we introduce a repulsive interaction between droplets across the film of thickness h *via*

$$v(h) = \alpha\gamma, \quad (11)$$

where α is the (dimensionless) interaction strength. If we assume that the particle–liquid–liquid contact line is fixed, we expect $\alpha \sim 1$. After all, the menisci between particles on the same droplet will undergo continued deformation upon draining of the interdroplet film (*i.e.* upon compression) for which the energy penalty per unit area is of the order of the liquid–liquid interfacial tension γ. If instead the contact angle is fixed, the contact line should slide along the particle surface, giving two additional contributions to the interaction energy: the change in (i) the wetted particle surface by the two liquid phases and (ii) the area of the oil–water interface. Both of these contributions are proportional to γ, so we can still write eqn (11), and they can easily be comparable to the contribution of the deformation of the liquid–liquid interface (ESI Section 9†). For $\alpha \sim 1$, the repulsive interaction in eqn (11) causes a Π-enhancement of approximately one order of magnitude (lines labelled '+PP' in Fig. 2).

Finally, we have considered the effects of droplet polydispersity, which have recently been studied in detail for surfactant-stabilized emulsions without finite interdroplet films ($h = 0$) by Maestro *et al.*[28] For monodisperse emulsions, they write

$$\frac{\Pi}{\gamma/R}(\phi) = K\frac{\phi^2(\phi - \phi_0)^{\beta-1}}{\sqrt{1-\phi}}, \quad (12)$$

in which $K = 3.64$ and $\beta = 2.5$. For polydisperse systems, they modify eqn (12) as follows

$$\frac{\Pi}{\gamma/R}(\phi) = K' z_c \beta\zeta\frac{\phi^2(\phi - \phi_0)^{\beta-1}}{\sqrt{1-\phi}}, \quad (13)$$

with $K' = 1.32$, z_c the number of first-neighbour contacts of a droplet,

$$z_c(\phi) \simeq 6 + 10\sqrt{\phi - \phi_0}, \quad (14)$$

$$\beta(z_c) \simeq 1.9 + 0.05 z_c, \quad (15)$$

and

$$\zeta(z_c) \simeq -0.016 + 0.0058 z_c. \quad (16)$$

Even though polydispersity does have an effect on the equation of state, this is much smaller than the effects of finite interdroplet films and repulsive interactions as described above, especially for $\phi \to 1$ (Fig. 2). Hence, it is unlikely that polydispersity can explain the observed Φ_{max}-reduction and Π-enhancement.

4 Results

4.1 Standard (opaque) emulsions

Prior to centrifugation, we characterized the structure of our samples using confocal microscopy, demonstrating that we had prepared w/o PR emulsions (Fig. 1). This observation is consistent with both sample composition and sedimentation behavior: water is the minority phase, the hydrophobic ($\theta \sim 160°$) particles prefer a continuous oil phase and the droplets are denser than *n*-dodecane. Qualitatively, it is clear from Fig. 3 that emulsions subjected to higher osmotic pressure Π (*i.e.* higher centrifugal acceleration) are compressed to higher droplet volume fraction Φ (*i.e.* more compact sediment). Note that the tops of the sediments are sometimes slanted, which we attribute to sample inhomogeneities rather than non-horizontal centrifugation (Fig. 1), as the latter should become less pronounced at higher centrifugal accelerations (contradicted by Fig. 3(b)).

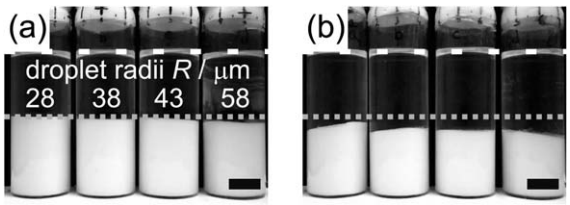

Fig. 3 Water-in-dodecane emulsions, stabilized by PMMA particles, ~8 min after centrifugation at (a) 33*g* and (b) 1289*g*. Scale bars 10 mm.

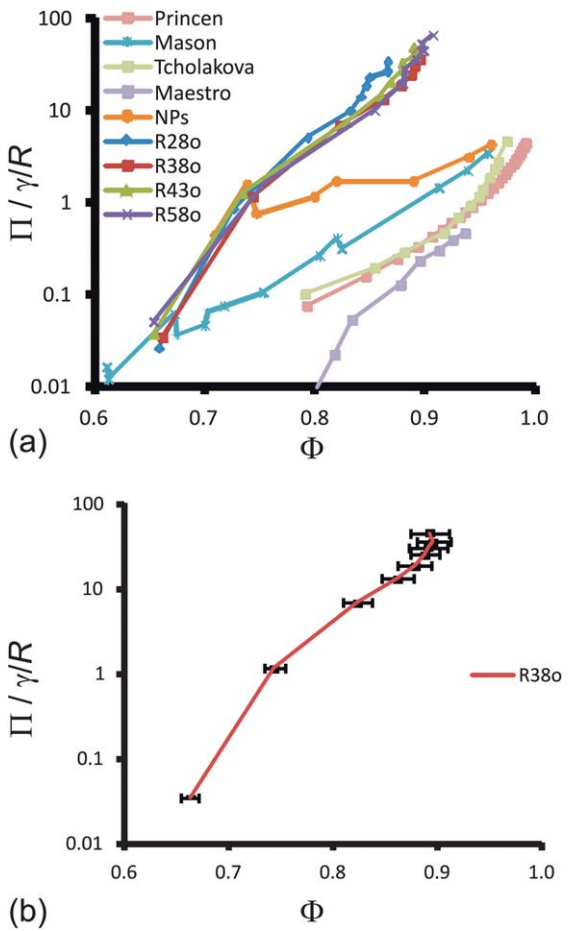

Fig. 4 (a) Symbols: measured osmotic pressure Π *vs.* droplet volume fraction Φ of emulsions stabilized by 0.630 μm radius PMMA particles ('R…o'), a molecular surfactant ('Princen', 'Mason', 'Tcholakova' and 'Maestro')[22,26–28] or flocculating nanoparticles (NPs).[13] R28o: mean droplet radius $R = 28$ μm in opaque sample, γ: corresponding liquid–liquid interfacial tension, solid lines are guides to the eye. (b) Measured (Π, Φ) – curve for R38o, including error bars instead of symbols (ESI Section 4†).

The Π (eqn (3)) *vs.* Φ (eqn (4)) data of four w/o PR emulsions with mean droplet radii R varying from 28 to 58 μm are shown in Fig. 4(a), which also includes literature data for emulsions stabilized by surfactants[22,26–28] and flocculating nanoparticles.[13] To allow a proper comparison between these data sets, they have been normalized by the appropriate value of the capillary pressure $P_c \propto \gamma/R$.[22,26,35] Whereas our results are comparable to the 'Mason' and 'NP' data sets at low Φ, they deviate substantially from all plotted literature data at high Φ, suggesting a previously undetected contribution from the stabilizing particles.

4.2 (Compound) transparent emulsions

After centrifugal compression, transparent samples were imaged in 3D at various locations along the cuvette (*i.e.* along the δ-axis in Fig. 1). Qualitatively, the micrographs in Fig. 5

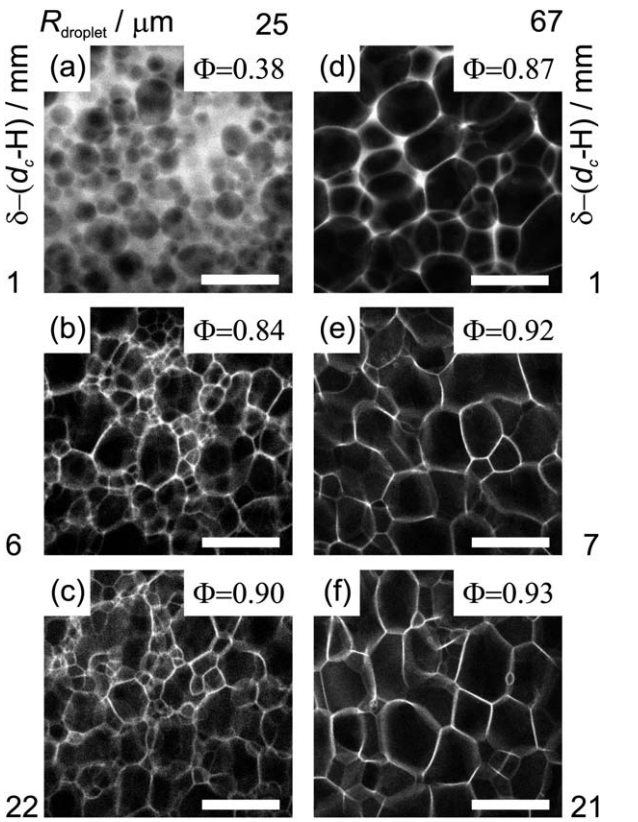

Fig. 5 Confocal fluorescence micrographs of two transparent water-in-oil (white) emulsions of droplet radius (a–c) 25 μm and (d–f) 67 μm, stabilized by 0.630 μm radius PMMA particles, at three different positions along the lever arm after centrifugation at ~263*g*. Taken from 3D image series at a depth of 200 μm. Scale bars (a–c) 100 μm and (d–f) 200 μm.

indicate that, except near the top of the sediment (Fig. 5(a/d)), Φ does not vary substantially across the sample, so our assumption of constant Φ for analyzing standard PR emulsions is partly justified (eqn (3) and Section 4.1). Note that our method for analyzing transparent PR emulsions does not assume a constant Φ along the sediment (Section 2.2).

Quantitatively, we use image analysis to extract Φ from image series taken from a depth of 100 μm to at least 300 μm. The corresponding graphs in Fig. 6(a) confirm that Φ is fairly constant along the sample apart from the top of the sediment, where $\Pi \sim 0$ by definition and so droplets may have moved upon tilting the sample horizontally for confocal imaging. Note that there seems to be a trend for emulsions with larger droplet sizes to have larger Φ_{max}, which is also predicted by our model (Section 3).

The spatial gradient in the centrifugal acceleration can be used to obtain an entire equation of state from one centrifugation cycle by employing eqn (2) to calculate $\Pi(\delta)$ *via* numerical integration of $\Phi(\delta)$ (Fig. 6). For clarity, we have only plotted $\Pi(\delta)$ *vs.* $\Phi(\delta)$ for two transparent samples (others in ESI Fig. 3†). Though the microscopy-derived curves are not quantitatively identical to the macroscopic ones (Fig. 6(b)), they are qualitatively similar, lending additional credibility to our methods. Note that the theory presented in Section 3 reproduces both the measured Φ_{max} and the observed Π-enhancement for $h = 7r$ and $\alpha = 1$ (dashed lines).

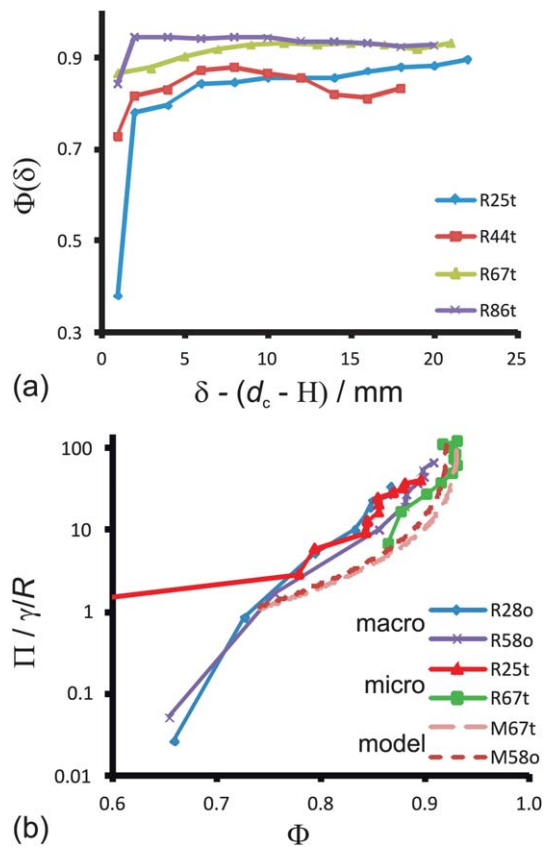

Fig. 6 (a) Droplet volume fraction Φ *vs.* distance to the top of the sediment in transparent PR emulsions, after centrifugation at ~263*g*. (b) Osmotic pressure Π *vs.* Φ of opaque and transparent PR emulsions from macroscopic and microscopic data; dashed lines calculated as described in Section 3 for $h = 4.4$ μm and $\alpha = 1$ ('M67t' is 'LL + FF + PP' in Fig. 2 and 'M58o' is the equivalent curve for $R = 58$ μm). All emulsions stabilized by 0.630 μm radius PMMA particles. Solid lines are guides to the eye, γ: interfacial tension, R67t: mean droplet radius $R = 67$ μm in transparent sample, macro data from Fig. 4.

5 Discussion

5.1 Equation of state

As predicted by our model (Fig. 2), our data features: (i) a relatively low Φ_{max}, and (ii) a Π-enhancement by about one order of magnitude (Fig. 4(a)), though we appreciate that the correspondence between theory and experiment is not perfect for all Φ. To explain the observed Φ_{max}, we have to set the interdroplet film thickness $h = 7r$, which is substantially larger than the thickness of a close-packed bilayer of interfacial particles ($h = 3.5r$). This actually corresponds well with confocal micrographs, which clearly show an additional layer of continuous oil phase in between the particle-coated droplets (Fig. 1 zoom).

This thicker interdroplet layer could be the result of emulsion recovery in the first 8 min after centrifugation, for which we have no recovery monitoring data. In addition, even though all supernatants were clear by eye after emulsification, we have observed some non-interfacial particles in micrographs of both types of emulsions (*e.g.* Fig. 1 zoom), which could contribute to thicker interdroplet films. Indeed, our model predicts that smaller particles should lead to higher Φ_{max}, which we have also observed (ESI Fig. 4†). Nanoparticles allow for even thinner interdroplet films, effectively because they have a larger surface-to-volume ratio, which results in even higher Φ_{max} (Fig. 4(a)). The lack of an upswing in Π at high Φ in the NP data suggests that these experiments simply have not probed the regime where the system exhibits an apparent divergence.

To explain the observed Π-enhancement (Fig. 4(a)), we have to set the dimensionless interaction strength $\alpha \sim 1$ (eqn (11)), which suggests that the effective repulsion between the droplets stems from the deformation of the liquid–liquid interface between particles on one droplet due to compression against a neighbouring droplet. In other words, the repulsion between droplets is due to a disjoining-pressure component that can be associated with the capillary stabilization of the interdroplet films by particles.[36] For example, if the three-phase contact line is fixed upon compression, the liquid–liquid interface between particles on the same droplet has to deform more upon draining of the interdroplet film, for which the energy penalty per unit area is of the order of the liquid–liquid interfacial tension γ. If instead the contact angle is constant, the contact line should slide along the particle surface, giving two additional contributions to the interaction energy: the change in (i) the wetted particle surface by the two liquid phases and (ii) the area of the oil-water interface. Both of these contributions are also proportional to γ and can easily be comparable to the contribution of the deformation of the liquid–liquid interface (ESI Section 9†).

Deformation of the liquid–liquid interface between interfacial particles on the same droplet should give rise to (attractive)

capillary forces between those particles.[11,12] To compare to interparticle interactions, we write eqn (11) as

$$v(h) = \alpha\gamma = \left(\frac{\varepsilon}{\pi r^2}\right) k_B T_0, \quad (17)$$

in which ε is a dimensionless interaction strength at the length scale of the particles. Our measurements indicate $\alpha \sim 1$, which means $\varepsilon \sim 1.5 \times 10^7$. Note that $\varepsilon k_B T_0 \lesssim \Delta G_d^{(max)} \sim 5.7 \times 10^7\ k_B T_0$ (minus sign in eqn (1) for removal into the water phase). This was to be expected, since additional deformation of the liquid–liquid interface between particles on the same droplet is equivalent to the particles being pushed into the aqueous droplet phase (which they do not prefer as $\theta \sim 160°$); we know $\varepsilon k_B T_0$ cannot greatly exceed $\Delta G_d^{(max)}$ (or particles would have been pushed off the interface). Indeed, an order of magnitude estimate for various potentially relevant interparticle interactions shows that only capillary forces can make a substantial contribution to the observed Π-enhancement (ESI Section 9 and 10†).

Now we would like to point out that the incomplete recovery of our PR emulsions (Section 5.2 below) suggests that we have not measured a thermodynamic (equilibrium) equation of state. However, we have performed our measurements following two different protocols, essentially with and without re-emulsification before centrifugation at a higher ω, both leading to similar results (ESI Section 5†). This suggests that our measurements are not very sensitive to the specific compression protocol used. In other words, we have measured the (pressure *vs.* density) equation of state *for the compression* of PR emulsions stabilized by hard-sphere particles.

5.2 Incomplete recovery

Intriguingly, the incomplete recovery of our PR emulsions, which allows for post-centrifugation characterization (Fig. 5), implies attractive forces between the droplets after compression.[35] One might be tempted to attribute these to zipping or bridging, *i.e.* particles on one droplet simultaneously adsorbing onto a second droplet,[37] which would indeed glue liquid–liquid interfaces together *via* shared particle monolayers.[38] To highlight any potential zipping, we repeated the centrifugal microscopy experiments with emulsions in which the particles were labeled with different fluorescent dyes. As exemplified in Fig. 7, we have not found any conclusive evidence for bridging (note the registering of red and green particles on adjacent interfaces). However, we have observed interfacial aggregates in the standard PR emulsions (ESI Fig. 2†, probably from incomplete particle dispersion), which may rotate onto the liquid–liquid interface upon compression, thereby 'locking in' the deformation – relaxation to a spherical droplet would require expelling interfacial particles, which is energy-expensive ($\Delta G_d \sim 6 \times 10^4\ k_B T_0$ per particle). Though interfacial aggregates probably do play a role in preventing droplet-shape relaxation, it cannot explain why the cells of our biliquid foams do not easily redisperse upon mechanical agitation (ESI Fig. 10(b)†).

Alternatively, droplet relaxation could be inhibited by attractive interactions between (interfacial) particles through the continuous phase. Though attractive interactions between

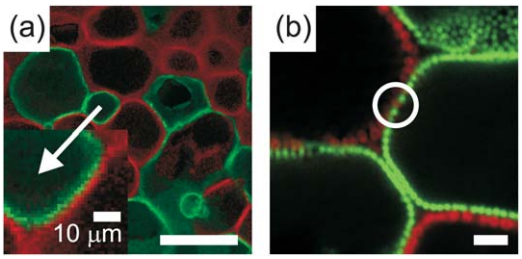

Fig. 7 Multicolor confocal fluorescence micrographs. (a) Water-in-dodecane emulsion, stabilized by micron-sized PMMA particles fluorescently labeled with NBD (green) or $DiIC_{18}$ (red), centrifuged at 362*g*. (b) Transparent emulsion, stabilized by micron-sized PMMA particles fluorescently labeled with NBD (green) or Rhodamine B (red), centrifuged at 838*g*. (b) The red circles are due to an optical artefact in long-working-distance objectives. The white circle highlights what looks like a zipping site, but we cannot rule out that it is caused by limited confocal resolution in the axial direction. Scale bars (a) 100 μm and (b) 10 μm.

PMMA–PHSA colloids in *n*-dodecane have been reported,[39] the majority of the evidence suggests that they are hard spheres in this and other hydrocarbon liquids.[23,24,40] These studies do not, however, rule out (osmotic) pressure-induced flocculation, *i.e.* they might flocculate due to strong compressive forces during centrifugation, analogous to film and cluster formation from colloidal suspensions upon diluent evaporation.[25,41]

To check the feasibility of pressure-induced flocculation, we estimate here the energy scale ΔG_c associated with centrifugal compression. ΔG_c should be of the same order as the (centrifugal) potential energy difference between two touching spheres at $\delta \sim d_c$ along the radial axis (Fig. 1),

$$\Delta G_c = m_{buoyant} a_c(d_c) \Delta\delta(d_c) = \left(\frac{4}{3}\pi r^3 (\rho_p - \rho_o)\right)(\omega^2 d_c)(2r). \quad (18)$$

This equates to 47.9 to $1.85 \times 10^3\ k_B T_0$ for 50.8 rad $s^{-1} \leq \omega \leq$ 316 rad s^{-1}. Values reported in the literature for repulsive free energies associated with steric barriers of PMMA–PHSA particles range from 75 to $3.4 \times 10^2\ k_B T_0$,[42] which can be overcome in the ω range calculated *via* eqn (18). In other words, the osmotic pressures applied in our experiments may well have pushed adjacent particles across their steric-stabilization barriers, thereby inhibiting post-centrifugation recovery. In addition, compression may lead to a relatively high density of steric polymer hairs in the interdroplet film, thereby increasing the effective viscosity of this film,[25] which can slow down its swelling after centrifugation by orders of magnitude.[43]

5.3 Materials-science aspects

Our results are clearly relevant for designing porous materials: we can control (i) the pore size *via* the initial droplet radius; (ii) the Plateau borders and volume fraction gradient *via* the applied pressure, and (iii) the interdroplet-film thickness *via* the particle radius. All of these features can be easily reproduced in a robust template *via* UV polymerization of a monomer/initiator mixture dissolved in the continuous phase.[14,44] Moreover, it is

important to know whether zipping occurs, since compressed but non-zipped particle-coated droplets do not necessarily form a continuous pathway in 3D (Fig. 7). Finally, the post-compression mechanical stability of these structures is crucial to their use as scaffolds for further processing. For example, we have observed that using poly (lauryl methacrylate) (PLMA) rather than PHSA as the stabilizer on the PMMA particles may result in post-centrifugation recoveries of $\gtrsim$65% rather than $\lesssim$10% (ESI Section 7†), which demonstrates that this choice is crucial for a well-controlled structure.

6 Conclusions

We have used centrifugal compression to measure the (pressure *vs.* density) equation of state of emulsions stabilized by hard-sphere colloids, thereby elucidating the contribution of the stabilizing particles. Moreover, we have presented results for a transparent model system, in which we have characterized volume-fraction gradients using confocal microscopy, allowing us to extract an entire equation of state from one centrifugation cycle. We have explained trends in our data using a quantitative model, which includes a finite interdroplet-film thickness and repulsive droplet facets; we suggest that the (effective) repulsion stems from the deformation of the liquid–liquid interface between particles on one droplet due to compression against a neighbouring droplet. Finally, we have discussed the incomplete post-centrifugation recovery of our Pickering emulsions and the relevance of predictive control to designing porous materials from particle-stabilized liquid–liquid composites, *e.g.* metal foams[45] and electrodes.[46]

Acknowledgements

We thank EPSRC EP/E030173/01 and EP/J007404/1 for financial support. M. E. C. is funded by the Royal Society and J. H. J. T. by the Royal Society of Edinburgh/BP Trust Personal Research Fellowship. The authors gratefully acknowledge O. Proctor & D. Wilson for preliminary experiments, T. Wood for the webcam software (labview), A. Imhof for his Mie scattering software *miescat*, the referees for stimulating suggestions and M. Hermes, D. Cheung & K. Velikov for useful discussions.

References

1 J. R. Seth, L. Mohan, C. Locatelli-Champagne, M. Cloitre and R. T. Bonnecaze, A micromechanical model to predict the flow of soft particle glasses, *Nat. Mater.*, 2011, **10**, 838–843.
2 M. D. Lacasse, G. S. Grest, D. Levine, T. G. Mason and D. A. Weitz, Model for the elasticity of compressed emulsions, *Phys. Rev. Lett.*, 1996, **76**, 3448–3451.
3 B. P. Binks and R. Murakami, Phase inversion of particle-stabilized materials from foams to dry water, *Nat. Mater.*, 2006, **5**, 865–869.
4 T. N. Hunter, R. J. Pugh, G. V. Franks and G. J. Jameson, The role of particles in stabilising foams and emulsions, *Adv. Colloid Interface Sci.*, 2008, **137**, 57–81.
5 J. W. Tavacoli, J. H. J. Thijssen, A. B. Schofield and P. S. Clegg, Novel, Robust, and Versatile Bijels of Nitromethane, Ethanediol, and Colloidal Silica: Capsules, Sub-Ten-Micrometer Domains, and Mechanical Properties, *Adv. Funct. Mater.*, 2011, **21**, 2020–2027.
6 B. P. Binks, Particles as surfactants – similarities and differences, *Curr. Opin. Colloid Interface Sci.*, 2002, **7**, 21–41.
7 J. H. J. Thijssen, A. B. Schofield and P. S. Clegg, How do (fluorescent) surfactants affect particle-stabilized emulsions?, *Soft Matter*, 2011, **7**, 7965–7968.
8 *CRC Handbook of Chemistry and Physics*, http://www.hbcpnetbase.com/, 2012, internet version.
9 A. D. Dinsmore, M. F. Hsu, M. G. Nikolaides, M. Marquez, A. R. Bausch and D. A. Weitz, Colloidosomes: selectively permeable capsules composed of colloidal particles, *Science*, 2002, **298**, 1006–1009.
10 M. Destribats, B. Faure, M. Birot, O. Babot, V. Schmitt and R. Backov, Tailored Silica Macrocellular Foams: Combining Limited Coalescence-Based Pickering Emulsion and Sol–Gel Process, *Adv. Funct. Mater.*, 2012, **22**, 2642–2654.
11 P. A. Kralchevsky, V. N. Paunov, I. B. Ivanov and K. Nagayama, Capillary Meniscus Interaction between Colloidal Particles Attached to a Liquid–Fluid Interface, *J. Colloid Interface Sci.*, 1992, **151**, 79–94.
12 P. A. Kralchevsky, V. N. Paunov, N. D. Denkov, I. B. Ivanov and K. Nagayama, Energetical and Force Approaches to the Capillary Interactions between Particles Attached to a Liquid–Fluid Interface, *J. Colloid Interface Sci.*, 1993, **155**, 420–437.
13 S. Arditty, V. Schmitt, F. Lequeux and F. Leal-Calderon, Interfacial properties in solid-stabilized emulsions, *Eur. Phys. J. B*, 2005, **44**, 381–393.
14 M. N. Lee, J. H. J. Thijssen, J. A. Witt, P. S. Clegg and A. Mohraz, Making a Robust Interfacial Scaffold: Bijel Rheology and its Link to Processability, *Adv. Funct. Mater.*, 2013, **23**, 417–423.
15 S. R. Waitukaitis and H. M. Jaeger, Impact-activated solidification of dense suspensions *via* dynamic jamming fronts, *Nature*, 2012, **487**, 205–209.
16 J. K. Ferri, P. Carl, N. Gorevski, T. P. Russell, Q. Wang, A. Boker and A. Fery, Separating membrane and surface tension contributions in Pickering droplet deformation, *Soft Matter*, 2008, **4**, 2259–2266.
17 S. Tcholakova, N. D. Denkov, I. B. Ivanov and B. Campbell, Coalescence in beta-lactoglobulin-stabilized emulsions: Effects of protein adsorption and drop size, *Langmuir*, 2002, **18**, 8960–8971.
18 N. Cheetangdee, M. Oki and K. Fukada, The Coalescence Stability of Protein-stabilized Emulsions Estimated by Analytical Photo-centrifugation, *J. Oleo Sci.*, 2011, **60**, 419–427.
19 C. P. Whitby, L. Lotte and C. Lang, Structure of concentrated oil-in-water Pickering emulsions, *Soft Matter*, 2012, **8**, 7784–7789.
20 D. Lerche and T. Sobisch, Direct and Accelerated Characterization of Formulation Stability, *J. Dispersion Sci. Technol.*, 2011, **32**, 1799–1811.

21 D. M. A. Buzza and M. E. Cates, Osmotic-Pressure of Dense Emulsion Systems – The Role of Double-Layer Forces, *Langmuir*, 1993, **9**, 2264–2269.
22 H. M. Princen and A. D. Kiss, Osmotic-Pressure of Foams and Highly Concentrated Emulsions. 2. Determination from the Variation in Volume Fraction with Height in an Equilibrated Column, *Langmuir*, 1987, **3**, 36–41.
23 G. Bosma, C. Pathmamanoharan, E. H. A. de Hoog, W. K. Kegel, A. van Blaaderen and H. N. W. Lekkerkerker, Preparation of monodisperse, fluorescent PMMA–latex colloids by dispersion polymerization, *J. Colloid Interface Sci.*, 2002, **245**, 292–300.
24 G. Bryant, S. R. Williams, L. Qian, I. K. Snook, E. Perez and F. Pincet, How hard is a colloidal "hard-sphere" interaction?, *Phys. Rev. E: Stat., Nonlinear, Soft Matter Phys.*, 2002, **66**, 060501.
25 *Dispersion Polymerization in Organic Media*, ed. K. E. J. Barrett, John Wiley & Sons, 1975.
26 T. G. Mason, J. Bibette and D. A. Weitz, Elasticity of Compressed Emulsions, *Phys. Rev. Lett.*, 1995, **75**, 2051–2054.
27 S. Tcholakova, N. D. Denkov, I. B. Ivanov and B. Campbell, Coalescence stability of emulsions containing globular milk proteins, *Adv. Colloid Interface Sci.*, 2006, **123**, 259–293.
28 A. Maestro, W. Drenckhan, E. Rio and R. Hoehler, Liquid dispersions under gravity: volume fraction profile and osmotic pressure, *Soft Matter*, 2013, **9**, 2531–2540.
29 X. Z. An, R. Y. Yang, K. J. Dong, R. P. Zou and A. B. Yu, Micromechanical simulation and analysis of one-dimensional vibratory sphere packing, *Phys. Rev. Lett.*, 2005, **95**, 205502.
30 A. I. Campbell and P. Bartlett, Fluorescent hard-sphere polymer colloids for confocal microscopy, *J. Colloid Interface Sci.*, 2002, **256**, 325–330.
31 D. R. Caudwell, J. P. M. Trusler, V. Vesovic and W. A. Wakeham, The viscosity and density of *n*-dodecane and *n*-octadecane at pressures up to 200 MPa and temperatures up to 473 K, *Int. J. Thermophys.*, 2004, **25**, 1339–1352.
32 B. E. Polat, S. Lin, J. D. Mendenhall, B. VanVeller, R. Langer and D. Blankschtein, Experimental and Molecular Dynamics Investigation into the Amphiphilic Nature of Sulforhodamine B, *J. Phys. Chem. B*, 2011, **115**, 1394–1402.
33 H. M. Princen, Osmotic-Pressure of Foams and Highly Concentrated Emulsions. 1. Theoretical Considerations, *Langmuir*, 1986, **2**, 519–524.
34 K. N. Nordstrom, E. Verneuil, W. G. Ellenbroek, T. C. Lubensky, J. P. Gollub and D. J. Durian, Centrifugal compression of soft particle packings: Theory and experiment, *Phys. Rev. E: Stat., Nonlinear, Soft Matter Phys.*, 2010, **82**, 041403.
35 V. G. Babak and M. J. Stebe, Highly concentrated emulsions: physicochemical principles of formulation, *J. Dispersion Sci. Technol.*, 2002, **23**, 1–22.
36 N. D. Denkov, I. B. Ivanov, P. A. Kralchevsky and D. T. Wasan, A Possible Mechanism of Stabilization of Emulsions by Solid Particles, *J. Colloid Interface Sci.*, 1992, **150**, 589–593.
37 K. P. Velikov, F. Durst and O. D. Velev, Direct observation of the dynamics of latex particles confined inside thinning water–air films, *Langmuir*, 1998, **14**, 1148–1155.
38 E. J. Stancik and G. G. Fuller, Connect the drops: using solids as adhesives for liquids, *Langmuir*, 2004, **20**, 4805–4808.
39 M. F. Hsu, E. R. Dufresne and D. A. Weitz, Charge stabilization in nonpolar solvents, *Langmuir*, 2005, **21**, 4881–4887.
40 P. A. Reynolds and C. A. Reid, Effect of Nonadsorbing Polymers on the Rheology of a Concentrated Nonaqueous Dispersion, *Langmuir*, 1991, **7**, 89–94.
41 G. R. Yi, V. N. Manoharan, E. Michel, M. T. Elsesser, S. M. Yang and D. J. Pine, Colloidal clusters of silica or polymer microspheres, *Adv. Mater.*, 2004, **16**, 1204–1208.
42 A. Doroszko and R. Lambourn, Measurement of Strength of Steric Barriers in Non-Aqueous Polymer Dispersions, *J. Polym. Sci., Polym. Symp.*, 1971, **34**, 253–264.
43 D. E. Tambe and M. M. Sharma, The Effect of Colloidal Particles on Fluid–Fluid Interfacial Properties and Emulsion Stability, *Adv. Colloid Interface Sci.*, 1994, **52**, 1–63.
44 J. H. J. Thijssen, A. V. Petukhov, D. C. 't Hart, A. Imhof, C. H. M. van der Werf, R. E. I. Schropp and A. van Blaaderen, Characterization of photonic colloidal single crystals by microradian X-ray diffraction, *Adv. Mater.*, 2006, **18**, 1662–1666.
45 J. Banhart, Manufacture, characterisation and application of cellular metals and metal foams, *Prog. Mater. Sci.*, 2001, **46**, 559–632.
46 X. Yang, P. He and Y. Xia, Preparation of mesocellular carbon foam and its application for lithium/oxygen battery, *Electrochem. Commun.*, 2009, **11**, 1127–1130.